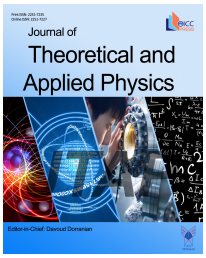

Volume 18, Issue 5, 182461 (1-11)

Journal of Theoretical and Applied Physics (JTAP)

https://dx.doi.org/10.57647/j.jtap.2024.1805.61

Reducing secondary particle dose in proton therapy for gastric tumors: a material optimization study

Nafise Asadi Jafari, Mojtaba Tajik*

School of Physics, Damghan University, Damghan, Iran.

***Corresponding author:** tajik@du.ac.ir

Original Research

Received:
27 July 2024
Revised:
31 August 2024
Accepted:
9 September 2024
Published online:
30 October 2024

© The Author(s) 2024

Abstract:

Proton therapy treats tumors by delivering high doses (in the form of Bragg peaks) to the target volume while protecting healthy tissue from radiation. However, secondary particles produce some dose, particularly neutrons, with high relative biological effects. This study used MCNPX code to investigate the impact of changing pre-collimator, snout, and diaphragm materials on the dose of secondary particles in proton therapy for gastric tumors. Results indicate that switching from brass to nickel reduces the total average dose of protons and secondary particles in most vital organs (excluding the tumor) by 44%. Additionally, the equivalent neutron dose to absorbed dose (H/D) in the brain decreased by 33%, and the average H/D in 14 vital organs dropped by approximately 12%. These findings demonstrate that changing collimator materials from brass to nickel can significantly reduce the harmful effects of secondary particle doses, particularly neutron doses, in gastric tumor treatment.

Keywords: Passive scattering proton therapy; Gastric tumor; Secondary particle dose; Collimator

1. Introduction

Research shows that proton therapy has been effective in the treatment of gastric cancer, which is the third leading cause of cancer death according to 2012 estimates [1–4]. Dionisi et al., Ted et al., and Verma et al. confirmed the use of proton therapy to treat gastric cancer [1, 2, 5]. Studies have shown that although proton therapy significantly reduces the initial dose of gastric cancer in healthy tissues, more research is needed in the field of secondary particle dosimetry and risk assessment for secondary cancers.

Among the secondary particles studied, the neutron dose can be concerning because it has higher values. In passive scattering radiotherapy, a scattering foil, adsorbent, and filters are used to broaden the Bragg peak (SOBP (spread out Bragg peak) formation) and obtain better tumor coverage [6, 7]. Passive scattering methods will continue to be used in the majority of proton therapy treatments [8–12], it is essential that we decrease the risks of secondary cancers caused on by neutron exposure. Through a simple modification to the collimator assembly design, our study shows that reaching this goal is achievable. However, patient-specific collimators are usually made of brass. The collimators are transferred to a designated storage location after treatment and remain there until their measured activity cannot be differentiated from the background. Then, they can be safely discarded. Because the cost of the materials used to make the apertures is high, alternative designs for lowering the cost without affecting the present clinical flow should be investigated [13].

In previous studies, the effect of the type of collimator has been presented only on the amount of neutron production [13–17], and the effect of changing the collimator due to the dose received by other body organs in treatment has not been investigated.

In this study, using the MCNPX code, the dose received by the involved and non-involved organs for stomach treatment was simulated for passive scattering proton therapy. Based on previous studies [18, 19], to reduce the risk of secondary cancers caused by secondary particles in the treatment of gastric cancer, the role of different collimator materials in reducing the dose of secondary particles, particularly neutrons, in the treatment of gastric cancer has been investigated.

Table 1. Specifications of materials that were investigated for collimators and pre-collimators [20].

Material name	Density (g/cm^3)	Thickness (cm)	Composition by mass used for Monte Carlo simulation
Brass	8.50	6.5	Copper (61.5%), Zinc (35.2%), Lead (3.3%)
Nickel	8.90	5.6	100% Ni

2. Materials

To study the effect of the pre-collimator material, snout, and diaphragm on the production of secondary particles, especially neutrons, as shown in Fig. 1, a dual scattering system of passive scattering proton therapy was considered [21]. Fig. 1 shows a double scattering nozzle whose components include: (A) the input of a proton beam in a vacuum, components, (B) range Modulation Wheel, and (C) a range-compensated scatter, to extend the input pencil beam to a wider radius for use in the treatment of tumors of various shapes and sizes, (D) a mid-base plate, and (E) a pre-collimator to remove proton scattered protons, which also supports the nozzle wall tube (F) Snout base-plate, (G) snout and (H) diaphragm, to eliminate protons outside the Planned Treatment Volume (PTV). These components are used to determine the shape of the final cross-section of the radiation field in the isocenter therapy [23]. The dimensions and compositions of the materials used in the Monte Carlo simulations are listed in Table 1. Using the SRIM program, the range corresponding to this beam in brass with a density of $\rho = 8.5$ gr/cm^3 and nickel with a density of $\rho = 8.9$ gr/cm^3 has been calculated to be 5.91 and 5.27 cm, respectively. Therefore, in the simulations, the thickness of collimators made of brass and nickel was considered to be 6.5 and 5.6 cm, respectively.

A directional point source was considered in the void, with an average proton beam energy of 231 MeV and a relative energy width of 0.26%. Water serves as an appropriate surrogate for tissues. Initially, simulations were conducted with the tumor positioned inside a water phantom. Subsequently, the simulation conditions were adjusted to more closely resemble the actual scenario by replacing the water phantom with the MIRD-UF phantom, which more accurately represents a human body. Fig. 1 illustrates the simple water phantom (containing the tumor) positioned in front of the proton therapy nozzle. The cylindrical phantom of water in the direction of the Z-axis had a diameter of 30 cm, and the tumor was considered as a cylinder with a diameter of 3 cm and a thickness of 1.5 cm inside it along the Z-axis from $-1.65 - -1.95$ cm. Since most gastric tumors are of the adenocarcinoma type ($90\% - 95\%$) [24], a tumor of this type was considered in the stomach wall of an adult male a Medical Internal Radiation Dose-University of Florida (MIRD-UF) phantom. In early gastric cancer, tumors less than 3 cm are classified as small tumors [25]. Therefore, a small tumor in the form of an elliptical cylinder with a thickness of 0.4 cm, a large diameter of 3 cm, and a small diameter of 1.5 cm, which is approximately 3.6 cm below the skin surface, was considered [4]. The composition of the substances in the tumor, taken from an article by Maughan et al. [22], is listed in Table 2. The depth of this tumor along the y-axis and the x-axis is from -1.22 to -2.72 cm and $6.5 - 9.5$ cm, respectively.

Fig. 2 shows the MIRD-UF phantom with a proton therapy nozzle. As shown in Fig. 2, the MIRD-UF phantom is exposed to single-proton energy. The Nozzle with Everything Upstream (NEU) program was developed by Bernard Gutschalk at Harvard University, who designed a double-scattering system [26, 27]. The treatment was performed using passive scattering in the NEU program [27]. Origin 2019 software packages were used to draw the simulation data in the form of diagrams.

2.1 Monte Carlo simulations

Because radiotherapy requires a pretreatment design and cannot be used as a test subject by the patient, computer simulations are used. Monte Carlo simulations provide an accurate method for test conditions [28]. Using the capabilities of the MCNPX code [21], the doses of protons and secondary particles produced in proton therapy for gastric cancer have been investigated and calculated. The effects of

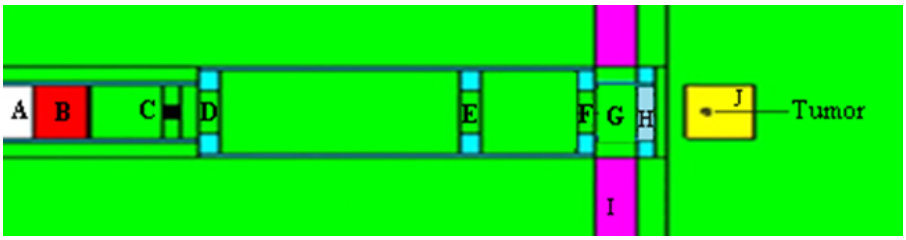

Figure 1. Geometry setup for the Monte Carlo simulation. View of the double scattering proton therapy nozzle, showing (A) Incoming uniform mono-energetic 231 MeV proton beam in a vacuum, (B) Range Modulation Wheel, (C) A range-compensated scatter, (D) A mid-base plate, (E) Pre-collimator, (F) Snout base-plate, (G) Snout, (H) Diaphragm, creating desired field shape and size (I) Concrete wall of the treatment room, (J) Water phantom in front of proton therapy nozzle.

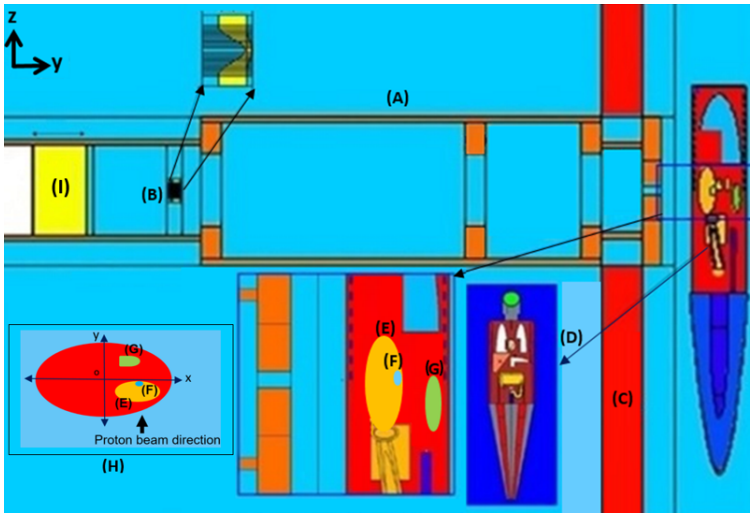

Figure 2. Geometry setup for the Monte Carlo simulation. MIRD-UF phantom with proton nozzle (A) the nozzle as described in Fig.1, (B) A range-compensated scatter, (C) concrete wall, (D) MIRD-UF phantom, (E) stomach, (F) tumor, (G) left kidney, (H) Cross-sectional area inside the phantom in the xy plane, (I) The 23rd step of the range modulation wheel.

different collimator materials on the depth dose, absorbed dose, and equivalent neutron dose in the phantoms of water and MIRD-UF were calculated.

The doses delivered by deuterons, tritons, ^{3}He, and heavier ions were much lower. They constitute approximately 1% or less of the absorbed therapeutic dose. Their energy and range are very low, and they discharge their kinetic energy alternately and very close to the point of their creation [29, 30]. Therefore, the dose of secondary particles, such as neutrons, photons, electrons, and positrons, was evaluated. The absorption doses of protons, electrons, and positrons were calculated using the tally F6. The absorbed dose obtained was expressed in terms of absorption energy per mass (MeV/g), which was multiplied by 1.602×10^{-10} to convert it to a unit (Gy/s). The energy deposition for the positron and the electron created by a proton interacting with an atom and a nucleus has been calculated using the FT card ELC option and the Electron Physics card. The FMn card was used to multiply the output by a fixed number to convert the absorbed dose unit from (MeV/g) to (Gy/s). The doses of transported neutrons and photon particles were calculated using the F4 tally card, and the equivalent dose was calculated using a dose function (DF) card. The flux-to-dose conversion factors were based on the ANSI/ANS -6.1.1-1977 report [31]. The equivalent dose obtained is expressed in Sv/h. To convert this unit to cSv/s, multiply by 2.778×10^{-2}. The FM card reports the output unit in cSv/s. In the MCNP code input file, the number of particle histories (NPS card) is set to 10×10^7. The maximum simulation error was approximately 1%.

3. Results

3.1 Distribution energy deposition of protons and secondary particles in tumor and adjacent organs

When protons are absorbed by a nucleus in an interaction, other particles leave the nucleus as products. These emitted particles such as protons, deuterons, lighter nuclei such as alpha and remaining recoiled nuclei, gamma photons, neutrons, electrons and positrons are called secondary particles. Each of these produced particles carries a part of the initial particle's energy [32].

The simulation results show that according to the depth of the tumor in the MIRD-UF phantom, which is in the direction of the y-axis from -1.22 to -2.72 cm, the 23rd step of the range modulation wheel is suitable for the formation of the Bragg peak. This step included 0.1199 cm of lead and 18.1331 cm of Lexan [21]. Based on this, a comparison was conducted between the water and MIRD-UF phantoms at the Bragg peak position based on this analysis.

In Fig. 3, the energy deposition curve in terms of penetration depth in the two phantoms of water and MIRD-UF has been compared. As seen in this figure, the location of the Bragg peak formation of the proton beam aligns with the geometry of the tumor. The protons in the phantom of water penetrate more into the tissue due to its lower density than the phantom MIRD-UF. The difference in the position of

Table 2. Percentage of elements in tumor tissue [22].

Type of tissue	Density (g cm^{-3})	K	S	P	Cl	Na	O	N	C	H
Adenocarcinoma tumor	1.04	0.36	0.54	0.36	0.36	0.18	56.9	4.5	26.9	9.9

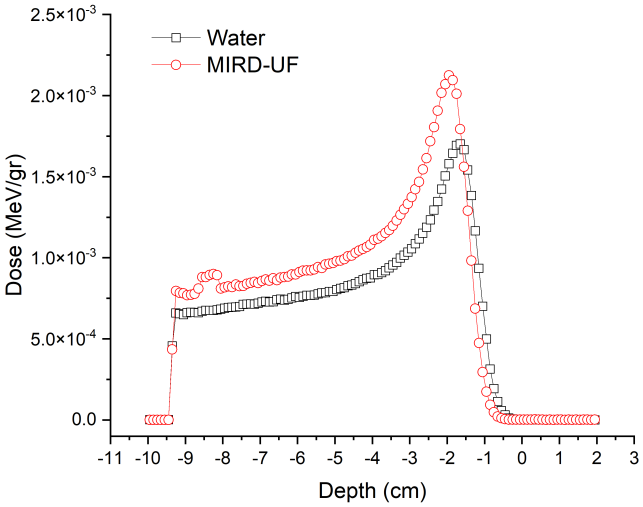

Figure 3. Energy deposition profiles in deep direction for the proton beam at different depths in the two phantoms of water and MIRD-UF for the collimators made of brass. The position of the tumour in Figs. 2 and 1 is in the direction of the Y-axis from -1.22 to -2.72 cm.

the Bragg peak in these two phantoms is about 3 mm. Also, energy deposition in the MIRD-UF phantom is higher than in the in the water phantom, which is related to the density difference between the two phantoms. The increased energy deposition around a depth of -8.35 cm is due to the presence of bone tissue from one of the ribs in the path of the proton beam. Since bone tissue is denser, it results in higher energy deposition. Therefore, in dosimetric calculations, water is used as a substitute for tissue; these changes need to be considered, especially in the case of small tumors where an error in determining the depth will damage healthy tissue.

In Figs. 4 (a) - (h), the distribution of energy deposited by proton particles in the tumor and energy deposited by secondary particles produced in the patient's body were calculated using a mesh tally card. The reference position (0 cm) of lateral distance in Fig. 4 is defined as the intersection of X and Y axes as shown in Fig. 4 (h). In these figures, the energy deposited by proton particles in the tumor and the energy deposited by secondary particles produced in the patient's body were qualitatively investigated for the two proton therapy systems. In the first system, the collimators were made of nickel, and in the second system, the collimators were made of brass. As shown in these figures, in the first system, the energy deposited by the protons in the tumor was greater than that in the second system, and the energy deposited by other secondary particles in the body was less for the first system than for the second system. Figs. 4 (a) and (b) show that proton particles leave almost all of their energy in the tumor. Figs. 4 (e) - (f) show that the photon energy, compared to other secondary particles, is distributed in a larger volume of the body. Figs. 4 (c) - (h) show that most of the energy deposition of secondary particles occurs in the skin and may cause allergies and skin diseases. Therefore, when treating a tumor, therapeutic and hygienic measures are necessary for the skin to reduce these risks [33].

The proton and secondary particle doses in the tumors and other healthy organs were calculated. The calculations are listed in Tables 3, 4, and Figs. 5 (a) - (d) have presented a comparison of the proton dose in other body organs except for the tumor for the nickel and brass collimators. The results listed in Tables 3, 4 show that the proton and secondary particle doses are reduced in the tumor and other tissues of the body by changing the material of the collimators from brass to nickel. Only the absorbed dose of protons in the left kidney and spleen as well as the absorbed positron dose in the brain and thyroid increased slightly, but the amount was negligible. The results shown in Figs. 5 (a) - (d) show that the use of nickel collimators instead of brass reduced the average proton dose by 18.8%, neutron dose by 6.2%, photon dose by 8.8%, and electron dose by 5% in the patient's body. The results shown in Fig. 5 (b) show that the neutron equivalent dose decreased in all organs of the body, except the left kidney and pancreas (which increased slightly). When secondary particles are produced, they may disperse in different directions after production, and the scattering of secondary particles, including neutrons, is greater in the left kidney and pancreas because of their proximity to the stomach.

3.2 Evaluation of neutron equivalent dose to the absorbed therapeutic dose (H/D) in tumors and vital organs

Another conventional calculation used to measure the secondary dose is the neutron equivalent dose to the absorbed therapeutic dose (H/D), where H is the equivalent neutron dose, and D is the absorbed dose of the proton in tumor [34]. Fig. 6 compares the H/D values within the tumor and organs of the body for a brass and nickel collimator. This figure shows that the H/D value is significantly reduced by changing the material of the collimators from brass to nickel. However, H/D values in the spleen, pancreas, and left kidney increased slightly. The percentage difference in H/D for the collimators made of brass and nickel was calculated according to Equation (1), where ε represents

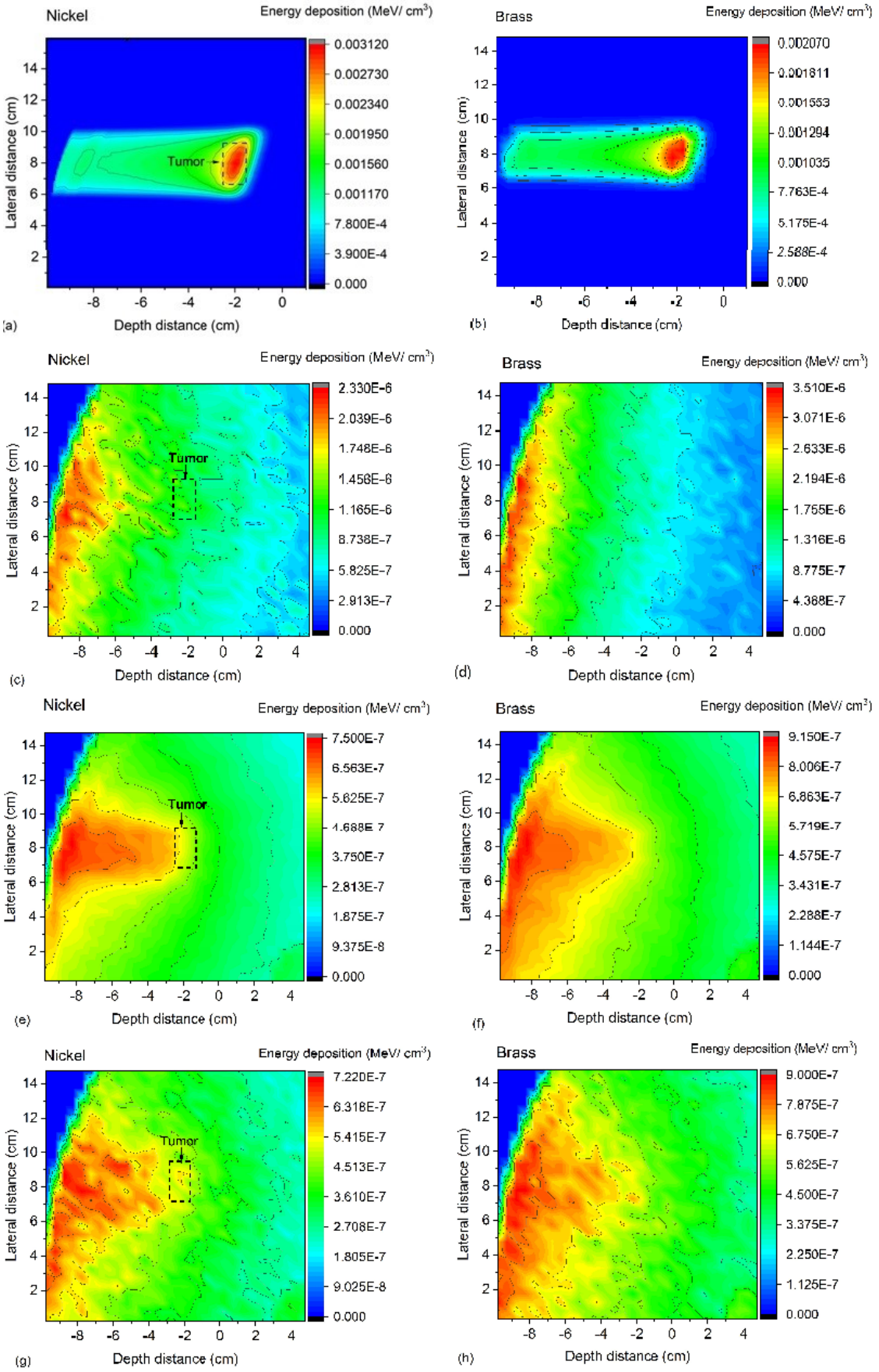

Figure 4. Monte Carlo simulated energy deposition in the tumor and other organs of the body for the collimators made of nickel (left), brass (right) for the particles of (a)-(b) proton; (c)-(d) neutron; (e)-(f) photon; and (g)-(h) electron.

Table 3. Calculated proton, electron and positron doses (Gy), and neutron and photon equivalent doses (cSv) in different organs of the MIRD-UF phantom with the collimators of nickel material.

Number organ	organ	Absorbed proton dose	Equivalent neutron dose	Equivalent photon dose	Absorbed electron dose	Absorbed positron dose
1	Tumor	83	143	0.86	0.00534	1.03E-4
2	Stomach	5.06	126	0.00645	1.49E-4	2.92E-6
3	Brain	3.83E-4	1.68	0.0168	7.47E-4	1.14E-5
4	Thyroid	0.0017	5.23	0.0523	0.0027	3.75E-5
5	Wall of the heart	0.0141	58.8	0.312	0.00245	3.48E-5
6	heart	0.0118	49.4	0.279	0.00202	2.05E-5
7	Left Kidney	0.0133	55.7	0.236	0.00153	2.44E-5
8	Right Kidney	0.0085	34.9	0.178	0.00218	2.82E-5
9	Liver	0.0106	44	0.25	0.00338	4.63E-5
10	Pancreas	0.0102	80.5	0.391	0.00249	3.73E-5
11	Spleen	0.0166	63.2	0.293	0.00234	2.98E-5
12	Bowel	0.0113	46.3	0.272	0.00126	2.97E-5
13	Skin	0.0087	32	0.153	0.00176	3.17E-5
14	Left lung	0.0102	41.9	0.204	1.26E-6	1.83E-5
15	Right lung	0.00574	24.1	0.145	0.00534	1.03E-4

Table 4. Calculated proton, electron and positron doses (Gy), and neutron and photon equivalent doses (cSv) in different organs of the MIRD-UF phantom with the collimators of brass material.

Number organ	organ	Absorbed proton dose (Gy)	Equivalent neutron dose (cSv)	Equivalent photon dose (cSv)	Absorbed electron dose (Gy)	Absorbed positron dose (Gy)
1	Tumor	83	145	1	0.00732	1.84E-4
2	Stomach	5.94	127	0.837	0.00699	1.06E-4
3	Brain	4.93E-4	1.85	0.0267	2.35E-4	2.5E-6
4	Thyroid	0.00173	6.39	0.0868	7.12E-4	8.63E-6
5	Wall of the heart	0.0163	67.97	0.488	0.00417	5.18E-5
6	Heart	0.014	57.32	0.442	0.00387	4.01E-5
7	Left Kidney	0.0126	52.81	0.367	0.00318	5.76E-5
8	Right Kidney	0.00908	35.88	0.289	0.00242	2.5E-5
9	Liver	0.0122	50.45	0.401	0.00341	4.24E-5
10	Pancreas	0.0486	79.73	0.584	0.00505	6.42E-5
11	Spleen	0.0157	66	0.448	0.00394	5.06E-5
12	Bowel	0.0122	51.43	0.44	0.00373	4.95E-5
13	Skin	0.0584	39.28	0.237	0.00194	3.99E-5
14	Left lung	0.0118	47.84	0.318	0.00287	4.48E-5
15	Right lung	0.00719	28.36	0.263	0.00201	2.5E-5

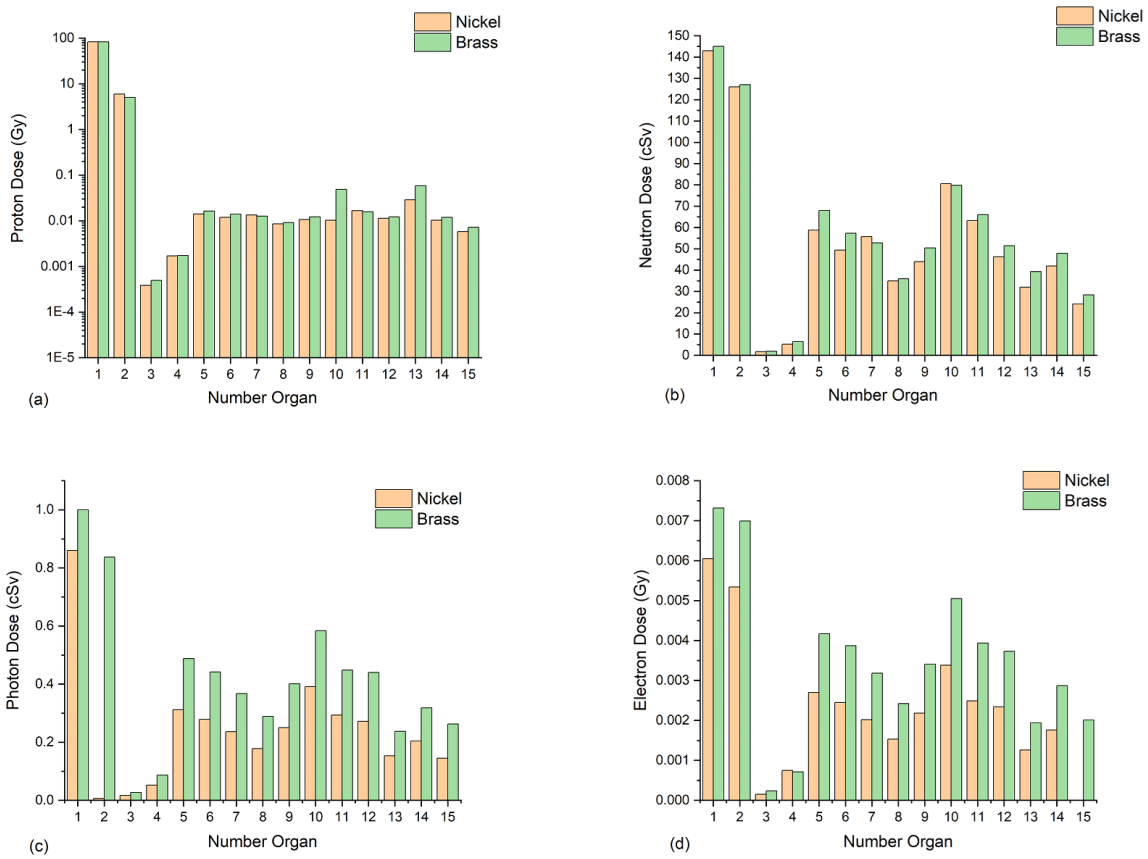

Figure 5. Monte Carlo simulated doses in the tumor and other organs of the body for the collimators made of nickel and brass for the particles of (a) proton, (b) neutron, (c) photon, and (d) electron. See Fig. 2 caption for geometry description.

the percentage difference in H/D for the nickel and brass collimators. The results of this calculation are shown in Fig. 6.

$$\varepsilon = \frac{(\mathrm{H/D})_{\mathrm{brass}} - (\mathrm{H/D})_{\mathrm{nickel}}}{(\mathrm{H/D})_{\mathrm{nickel}}} \qquad (1)$$

The results in Fig. 6 show that the highest relative H/D difference (reduction) was 33% in the brain, 22% in the skin and thyroid, 15% in the heart, and 18% in the right lung.

These results show the extent to which the change of collimators from brass to nickel can play a role in reducing the possible destructive effects of the secondary particle dose, especially the neutron dose, in the organs of the body. When a nickel collimator is used instead of brass, the calculations show that the average H/D in all vital organs is reduced by approximately 11.5%.

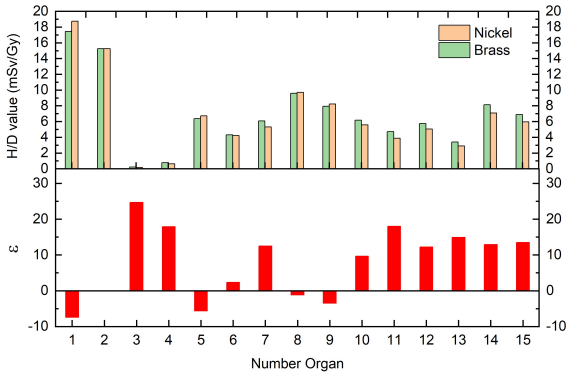

Figure 6. Equivalent neutron dose to therapeutic absorbed dose (H/D) from neutrons produced by mono-energetic 231 MeV protons, in body organs and relative H/D difference (ε) for the collimators made of nickel and brass.

4. Discussion

Tables 3 and 4 show that high secondary neutron dose levels can be recorded in vital structures such as untreated stomach, healthy brain tissue, etc., and these should be considered in clinical practice. In addition, the tables also show that organs far from the treatment field, such as the brain and thyroid, receive a lower neutron dose compared to organs near the treatment field, such as the heart and pancreas. The results of this study are comparable to the results of Farah and his colleagues, who used the MCNPX code to investigate secondary neutron doses in proton therapy of eye melanoma and craniopharyngioma [35]. They showed that the organs adjacent to the tumor receive a high dose of neutrons compared to the healthy organs further away from the radiation field.

In a separate study conducted by Fontenot et al., a prostate treatment using a 250 MeV passive technique was examined, and the authors reported neutron equivalent doses [36]. The study revealed that the closest organ to the treatment field (bladder) received a significantly higher equivalent dose per therapeutic (H/D) of 12 mSv Gy^{-1}, while the farthest organ (esophagus) received a lower H/D of 1.9 mSv Gy^{-1}. These findings are consistent with the results of Fontenot's study. The stomach, positioned closest to the treatment field, received a H/D of 17 mSv Gy^{-1}, whereas the brain, located furthest from the treatment field, received a H/D of 0.2 mSv Gy^{-1}.

The results of this study align with those of Agosteo et al., who utilized the FLUKA code to investigate neutron and photon doses in proton therapy for eye tumors [37]. The authors demonstrated that in a passive scattering proton system, the maximum estimated dose resulting from secondary particles ranged from 10^{-4} to 10^{-2} Gy per therapy Gy. Furthermore, the study results indicate that the dose of secondary particles in non-involved organs is comparatively lower, ranging from 10^{-5} to 10^{-3} Gy per therapy Gy, when compared to the findings reported by Agosteo and colleagues.

The results of this study are comparable to those of Brenner et al., who used the MCNPX code to model the transport of a uniform flux of monoenergetic 235 MeV protons affecting on the pre-collimator and patient-specific collimator [20]. The researchers specifically focused on calculating the patient dose resulting from neutrons originating in a pre-collimator and collimator configuration, per proton collision on the collimator plate. Their study demonstrated that in cases where both the pre-collimator and collimator were metallic, the use of nickel as the material compared to brass resulted in lower production of secondary neutron doses. In other words, nickel collimators exhibited improved performance in terms of reducing the production of secondary neutron doses. In a study by Jason Holmes et al., the authors introduce the Spot Scanning Aperture (SSA), a novel device concept developed to precisely collimate individual proton beamlets during radiation therapy [38]. The SSA's dosimetric properties were evaluated, showing significant improvements in spot size reduction and dose distribution at shallow depths, with findings dependent on aperture material and thickness. The study compared neutron doses produced by different aperture materials (tungsten, lead, brass, and nickel) when protons pass through them. Tungsten produced the highest neutron dose, while nickel produced the lowest. The results of this study, similar to those of Jason et al., indicate that the dose of secondary particles, especially neutrons, is lower for a collimator made of nickel compared to brass. The choice of aperture material is crucial for minimizing neutron dose in proton therapy, with nickel being the preferred material due to its lower neutron production. In addition to collimator materials, other factors such as beam energy, patient anatomy, and advanced treatment planning techniques like spot-scanning diaphragms (SSAs) can also influence dose distribution [38].

Secondary cancers can develop as a long-term consequence of radiation therapy due to the exposure of healthy tissues to scattered or unintended radiation. By minimizing this exposure with the use of nickel collimators, the likelihood of DNA damage in these healthy cells is reduced. Over time, this can lower the risk of developing secondary malignancies, particularly in younger patients who have a longer life expectancy after treatment. Radiation-induced side effects, such as fibrosis, necrosis, or damage to critical organs (like the heart or lungs when treating chest tumors), are directly related to the dose of radiation received by these tissues. By reducing the dose with the help of precise collimation, the risk of these adverse effects is also lowered, leading to better overall patient outcomes and quality of life post-treatment. Nickel collimators offer better beam collimation, improved durability, reduced secondary neutron production, and superior corrosion resistance compared to brass collimators in proton therapy. These advantages contribute to more precise and safer cancer treatments, making nickel a preferred material in many cases. Brass collimators in proton therapy offer cost savings, ease of machining, non-magnetic properties, and good durability in appropriate environments. These advantages make brass a viable option, particularly when cost, non-magnetic requirements, and ease of fabrication are prioritized. However, the choice between nickel and brass may also depend on specific treatment requirements, cost considerations, and the magnetic environment of the therapy system.

5. Conclusion

The simulation results showed that by changing the collimator material from brass to nickel, the equivalent neutron and photon doses and the absorbed electron dose decreased in almost all body organs. Since it is an ideal treatment in which the secondary particle dose is very low to prevent the recurrence of cancer, according to the results obtained, among the studied materials, nickel is a better option than brass for use in the proton therapy system. In future research, the impact of changes in the patient's anatomy or tumor location on the effectiveness of nickel collimators could be explored, potentially leading to more personalized and effective treatment plans. Additionally, the environmental and safety aspects of using various materials, especially nickel, could be examined in future research.

Authors contributions
Nafise Asadi Jafari: Software, Validation, Formal analysis, Investigation, Data curation, Visualization. Mojtaba Tajik: Conceptualization, Methodology, Software, Validation, Formal analysis, Investigation, Data curation, Writing-Original draft preparation, Writing-Reviewing and Editing, Supervision, Project administration.

Availability of data and materials
The data that support the findings of this study are available from the corresponding author upon reasonable request.

Conflict of interests
The authors declare that they have no known competing financial interests or personal relationships that could have appeared to influence the work reported in this paper.

Open access
This article is licensed under a Creative Commons Attribution 4.0 International License, which permits use, sharing, adaptation, distribution and reproduction in any medium or format, as long as you give appropriate credit to the original author(s) and the source, provide a link to the Creative Commons license, and indicate if changes were made. The images or other third party material in this article are included in the article's Creative Commons license, unless indicated otherwise in a credit line to the material. If material is not included in the article's Creative Commons license and your intended use is not permitted by statutory regulation or exceeds the permitted use, you will need to obtain permission directly from the OICC Press publisher. To view a copy of this license, visit https://creativecommons.org/licenses/by/4.0.

References

[1] F. Dionisi, S. Avery, J. N. Lukens, X. Ding, J. Kralik, M. Kirk, R. E. Roses, M. Amichetti, J. M. Metz, and J. P. Plastaras. "Proton therapy in adjuvant treatment of gastric cancer: Planning comparison with advanced x-ray therapy and feasibility report.". *Acta Oncologica*, **53**:1312–1320, 2014. DOI: https://doi.org/10.3109/0284186X.2014.912351.

[2] T. C. Ling, J. I. Kang, J. D. Slater, and G. Y. Yang. "Proton therapy for gastrointestinal cancers.". *Translational Cancer Research (Particle Beam Therapy I)*, **1**, 2012. DOI: https://doi.org/10.3978/j.issn.2218-676X.2012.09.01.

[3] S. Koyama, N. Kawanishi, H. Fukutomi, T. Osuga, T. Iijima, H. Tsujii, and T. Kitagawa. "Advanced carcinoma of the stomach treated with definitive proton therapy.". *Am J Gastroenterol*, **85**:443–447, 1990.

[4] S. Shibuya, Y. Takase, H. Aoyagi, K. Orii, N. Sharma, H. Tsujii, H. Tsuji, and Y. Iwasaki. "Definitive proton beam radiation therapy for inoperable gastric cancer: a report of two cases.". *Radiation Medicine*, **9**:35–40, 1991.

[5] V. Verma, S. H. Lin, C. B. Simone, and M. P. Mehta. "Clinical outcomes and toxicities of proton radiotherapy for gastrointestinal neoplasms: a systematic review.". *Journal of Gastrointestinal Oncology*, **7**:644, 2016. DOI: https://doi.org/10.21037/jgo.2016.05.06.

[6] P. J. Taddei, J. D. Fontenot, Y. Zheng, D. Mirkovic, A. K. Lee, U. Titt, and W. D. Newhauser. "Reducing stray radiation dose to patients receiving passively scattered proton radiotherapy for prostate cancer.". *Physics in Medicine & Biology*, **53**:2131, 2008. DOI: https://doi.org/10.1088/0031-9155/53/8/009.

[7] M. F. Moyers, E. R. Benton, A. Ghebremedhin, and G. Coutrakon. "Leakage and scatter radiation from a double scattering based proton beamline. ". *Med Phys*, **35**:128–144, 2008. DOI: https://doi.org/10.1118/1.2805086.

[8] J. A. Bradley, M. W. Ho, Z. Li, X. Liang, M. Rutenberg, R. Dagan, and N. P. Mendenhall. "A technical guide for passive scattering proton radiation therapy for breast cancer.". *International Journal of Particle Therapy*, **3**:473–484, 2017. DOI: https://doi.org/10.14338/IJPT-16-00025.1.

[9] M. H. Abu-Arja, A. L. Brown, J. M. Su, M. F. Okcu, H. B. Lindsay, S. L. McGovern, M. F. McAleer, D. R. Grosshans, M. M. Chintagumpala, and A. C. Paulino. "The cochlear dose and the age at radiotherapy predict severe hearing loss after passive scattering proton therapy and cisplatin in children with medulloblastoma.". *Neuro-Oncology*, **114**:38916058, 2024. DOI: https://doi.org/10.1093/neuonc/noae114.

[10] M. Takagi, Y. Hasegawa, K. Tateoka, Y. Takada, and M. Hareyama. "Dosimetric comparison study of proton therapy using line scanning versus passive scattering and volumetric modulated Arc therapy for localized prostate cancer.". *Cancers*, **16**:4.3, 2024. DOI: https://doi.org/10.3390/cancers16020403.

[11] Y. Mori, T. Isobe, H. Takei, S. Kamizawa, T. Tomita, D. Kobayashi, H. Sakurai, and T. Sakae. "The impact of dose calibration point differences between the treatment plan and patient-specific quality assurance in passive scattering proton beam therapy.". *In vivo (Athens, Greece)*, **38**:2478–2483, 2024. DOI: https://doi.org/10.21873/invivo.13718.

[12] Y. Tominaga, M. Suga, M. Takeda, Y. Yamamoto, T. Akagi, T. Kato, S. Tokumaru, M. Yamamoto, and M. Oita. "Dose-volume comparisons of proton therapy for pencil beam scanning with and without multi-leaf collimator and passive scattering in patients with lung cancer.". *Medical Dosimetry*, **49**:13–18, 2024. DOI: https://doi.org/10.1016/j.meddos.2023.10.006.

[13] H. Chen, W. Matysiak, S. Flampouri, R. Slopsema, and Z. Li. "Dosimetric evaluation of hybrid brass/stainless-steel apertures for proton therapy.". *Phys Med Biol*, **59**:5043–5060, 2014. DOI: https://doi.org/10.1088/0031-9155/59/17/5043.

[14] A. Cesana, E. Mauro, and M. Silari. "Induced radioactivity in a patient-specific collimator used in proton therapy.". *Nuclear Instruments and Methods in Physics Research Section B: Beam Interactions with Materials and Atoms*, **268**:2272–2280, 2010.

[15] E. S. Diffenderfer, C. G. Ainsley, M. L. Kirk, J. E. McDonough, and R. L. Maughan. "Comparison of secondary neutron dose in proton therapy resulting from the use of a tungsten alloy MLC or a brass collimator system.". *Med Phys*, **38**:6248–6256, 2011. DOI: https://doi.org/10.1118/1.3656025.

[16] B. Gustafsson. "Optimization of material in proton-therapy collimators with respect to neutron production. ". , 2009.

[17] R. Tayama, Y. Fujita, M. Tadokoro, H. Fujimaki, T. Sakae, and T. Terunuma. "Measurement of neutron dose distribution for a passive scattering nozzle at the Proton Medical Research Center (PMRC).". *Nuclear Instruments and Methods in Physics Research Section A: Accelerators, Spectrometers, Detectors and Associated Equipment*, **564**:532–536, 2006. DOI: https://doi.org/10.1016/j.nima.2006.04.028.

[18] D. J. Brenner and E. J. Hall. "Secondary neutrons in clinical proton radiotherapy: a charged issue.". *Radiotherapy and Oncology*, **86**:165–170, 2008. DOI: https://doi.org/10.1016/j.radonc.2007.12.003.

[19] X. G. Xu, B. Bednarz, and H. Paganetti. "A review of dosimetry studies on external-beam radiation treatment with respect to second cancer induction.". *Physics in Medicine & Biology*, **53**:R193, 2008. DOI: https://doi.org/10.1088/0031-9155/53/13/R01.

[20] D. J. Brenner, C. D. Elliston, E. J. Hall, and H. Paganetti. "Reduction of the secondary neutron dose in passively scattered proton radiotherapy, using an optimized pre-collimator/collimator. ". *Physics in Medicine & Biology*, **54**:6065, 2009. DOI: https://doi.org/10.1088/0031-9155/54/20/003.

[21] J. M. Ryckman. "Using MCNPX to calculate primary and secondary dose in proton therapy.". , 2011.

[22] R. L. Maughan, P. Chuba, A. T. Porter, E. Ben-Josef, D. R. Lucas, and B. E. Bjarngard. "Mass energy-absorption coefficients and mass collision stopping powers for electrons in tumors of various histologies.". *Medical Physics*, **26**:472–477, 1999. DOI: https://doi.org/10.1118/1.598544.

[23] L. Grevillot. "Monte Carlo simulation of active scanning proton therapy system with Gate/Geant4: Towards a better patient dose quality assurance. ". , 2011.

[24] B. Dent and S. M. Griffin. "Gastric tumours.". *Surgery (Oxford)*, **32**:608–613, 2014. DOI: https://doi.org/10.1016/j.mpsur.2014.09.002.

[25] W. J. Im, M. G. Kim, T. K. Ha, and S. J. Kwon. "Tumor size as a prognostic factor in gastric cancer patient. ". *Journal of Gastric Cancer*, **12**:164–172, 2012. DOI: https://doi.org/10.5230/jgc.2012.12.3.164.

[26] B. Gottschalk. "NEU User Guide. ". *Laboratory for Particle Physics and Cosmology*, , 2006.

[27] B. Gottschalk. "NEU Codes Package.". , 2017.

[28] F. Fracchiolla and M. Schwarz. "Improving the quality of protontherapy treatment plans and their verification with Monte Carlo methods. ". *Physica Medica: European Journal of Medical Physics*, **32**:23, 2016. DOI: https://doi.org/10.1016/j.ejmp.2016.01.080.

[29] Y. D. H. Matsuzaki, K. L. Sutherland, and Y. Kiyanagi. "Nuclear collision processes around the Bragg peak in proton therapy.". *Radiol Phys Technol.*, **3**:84–92, 2010. DOI: https://doi.org/10.1007/s12194-009-0081-2.

[30] W. D. Newhauser and R. Zhang. "The physics of proton therapy.". *Physics in Medicine & Biology*, **60**:R155, 2015. DOI: https://doi.org/10.1088/0031-9155/60/8/R155.

[31] American Nuclear Society. "Working Group ANS: American national standard neutron and gamma-ray flux-to-dose-rate factors: American Nuclear Society". , 1977.

[32] M. J. Berger. "Penetration of proton beams through water 1. Depth-dose distribution, spectra and LET distribution: US Department of Commerce.". *National Institute of Standards and Technology*, , 1993.

[33] G. Mondlane, A. N. A. Ureba, M. Gubanski, P. A. Lind, and A. Siegbahn. "Estimation of risk of normal-tissue toxicity following gastric cancer radiotherapy with photon- or scanned proton-beams.". *Anticancer Research*, **38**:2619, 2018. DOI: https://doi.org/10.21873/anticanres.12503.

[34] Y. Zheng, W. Newhauser, J. Fontenot, P. Taddei, and R. Mohan. "Monte Carlo study of neutron dose equivalent during passive scattering proton therapy.". *Physics in Medicine & Biology*, **52**:4481, 2007. DOI: https://doi.org/10.1088/0031-9155/52/15/008.

[35] J. Farah, R. Sayah, F. Martinetti, L. Donadille, V. Lacoste, J. Hérault, S. Delacroix, C. Nauraye, I. Vabre, C. Lee, et al. "Secondary neutron doses in proton therapy treatments of ocular melanoma and craniopharyngioma.". *Radiation Protection Dosimetry*, **161**:363–367, 2014. DOI: https://doi.org/10.1093/rpd/nct283.

[36] J. Fontenot, P. Taddei, Y. Zheng, D. Mirkovic, T. Jordan, and W. Newhauser. "Equivalent dose and effective dose from stray radiation during passively scattered proton radiotherapy for prostate cancer.". *Physics in Medicine & Biology*, **53**:1677, 2008. DOI: https://doi.org/10.1088/0031-9155/53/6/012.

[37] S. Agosteo, C. Birattari, M. Caravaggio, M. Silari, and G. Tosi. "Secondary neutron and photon dose in proton therapy. ". *Radiotherapy and Oncology*, **48**: 293–305, 1998. DOI: https://doi.org/10.1016/S0167-8140(98)00049-8.

[38] J. Holmes, J. Shen, S. H. Patel, W. W. Wong, R. L. Foote, M. Bues, and W. Liu. "Collimating individual beamlets in pencil beam scanning proton therapy, a dosimetric investigation.". *Frontiers in Oncology*, **12**:1031340, 2022. DOI: https://doi.org/10.3389/fonc.2022.1031340.